Earthquakes and Structures, *Vol. 18, No. 5 (2020)599-607*
DOI: https://doi.org/10.12989/eas.2020.18.5.599

Seismic performance of RCS beam-column joints using fiber reinforced concrete

Xuan Huy Nguyen*[1], Dang Dung Le[1a], Quang-Huy Nguyen[2b] and Hoang Quan Nguyen[1c]

[1]Faculty of Construction Engineering, University of Transport and Communications, Vietnam
[2]Department of Civil Engineering and Urban Planning, INSA de Rennes, France

(*Received January 20, 2020, Revised March 16, 2020, Accepted April 12, 2020*)

Abstract. This paper deals with the experimental investigation on the behavior of RCS beam-column exterior joints. Two full-scale specimens of joints between reinforced concrete columns and steel beams are tested under cyclic loading. The objective of the test is to study the effect of steel fiber reinforced concrete (SFRC) on the seismic behavior of RCS joints. The load bearing capacity, story drift capacity, ductility, energy dissipation, and stiffness degradation of specimens are evaluated. The experimental results point out that the FRC joint is increased 20% of load carrying capacity and 30% of energy dissipation capacity in comparison with the RC joint. Besides, the FRC joint shown lower damage and better ductility than RC joint.

Keywords: RCS joint; steel fiber reinforced concrete; cyclic load; seismic behavior

1. Introduction

Reinforced concrete- steel (RCS) moment frame structures are composed by reinforced concrete (RC) columns and steel (S) beams. This type of composite structures has gained increasingly attention in the past few decades because it has several advantages in comparison with either traditional RC frames or steel frames in terms of structural, economical and constructional viewpoints (Nishiyama *et al.* 2004, Jinjie *et al.* 2015, Li *et al.* 2016). One of the most challenging parts in design of RCS frames is the connection between RC column and steel beam. Therefore, there are many studies about the behavior of composite RCS beam–column connections (Deierlein *et al.* 1989, Fargier-Gabaldon 2005, Dong *et al.* 2018, Mirghaderi *et al.* 2016, Nguyen *et al.* 2019, Zhang *et al.* 2018). For instance, experiments were conducted by Deierlein *et al.* (1989) to identify the in-plane behavior of RCS beam-column connections. Based on this valuable work, the American Society of Civil Engineers (ASCE Task Committee 1994) has developed the design guidelines for both interior and exterior RCS joints in buildings located in low to moderate seismic risk zones. Another experimental program was run by Kanno and Deierlein (2002) using a series of 19 interior RCS joint specimens tested under the cyclic loading. Their objective was to investigate joint failure modes, the performance of high strength concrete joints, the joint aspect ratio, and the effect of column axial load on joints. Experimental results of nine exterior RCS connections presented by Parra-Montesinos *et al.* (2010) also emphasized that RCS frames were suitable for use in high seismic risk zones. An exterior RCS joint, in which a steel profile inside RC column is directly welded to the steel beam, has been recently presented in European project SmartCoCo (Smart Composite Components). The most important advantage of this hybrid joint is to create an easy and simple connection between steel beams and RC columns. Furthermore, such connection improves the capability of energy dissipation and the ductility of structures in comparison with the joint between steel beams and RC columns without embedded steel profiles. An experimental study on cyclic behavior of this joint conducted by Nguyen *et al.* (2018) showed that it can be used as dissipative elements in medium ductility structures. However, this study has the weakness in practical deployment because the joint requires a complex design of stirrups in the connection zone. This leads to the congestion of reinforcement and difficulties in placing and consolidating the concrete in the connection zone. This problem has led to developing the new method using fiber reinforced concrete (FRC) to improve the structural performance (Gong *et al.* 2018, Oinam *et al.* 2019).

There were many studies using FRC in beam - column joints to reduce the reinforcement concentration and to improve the seismic performance. Kalaivani *et al.* (2016) has summarized existing studies on behavior of steel fiber reinforced concrete beam – column joint. The review paper has drawn the conclusion that the presence of steel fiber in concrete helped to reduce the crack width and damages to the specimen. Furthermore, the SFRC beam - column joints increased the ultimate load carrying capacity, stiffness, ductility and energy absorption capacity than those of conventional RC specimens. For example, Gefken and Ramey (1989) investigated the performance of exterior beam - column joints by using SFRC and increasing stirrup distances to 1.7 times of recommended distances for joints.

*Corresponding author, Associate Professor
E-mail: nguyenxuanhuy@utc.edu.vn
[a]Ph.D. Student
[b]Associate Professor
[c]Ph.D.

http://www.techno-press.com/journals/was&subpage=7
ISSN: 2092-7614 (Print), 2092-7622 (Online)

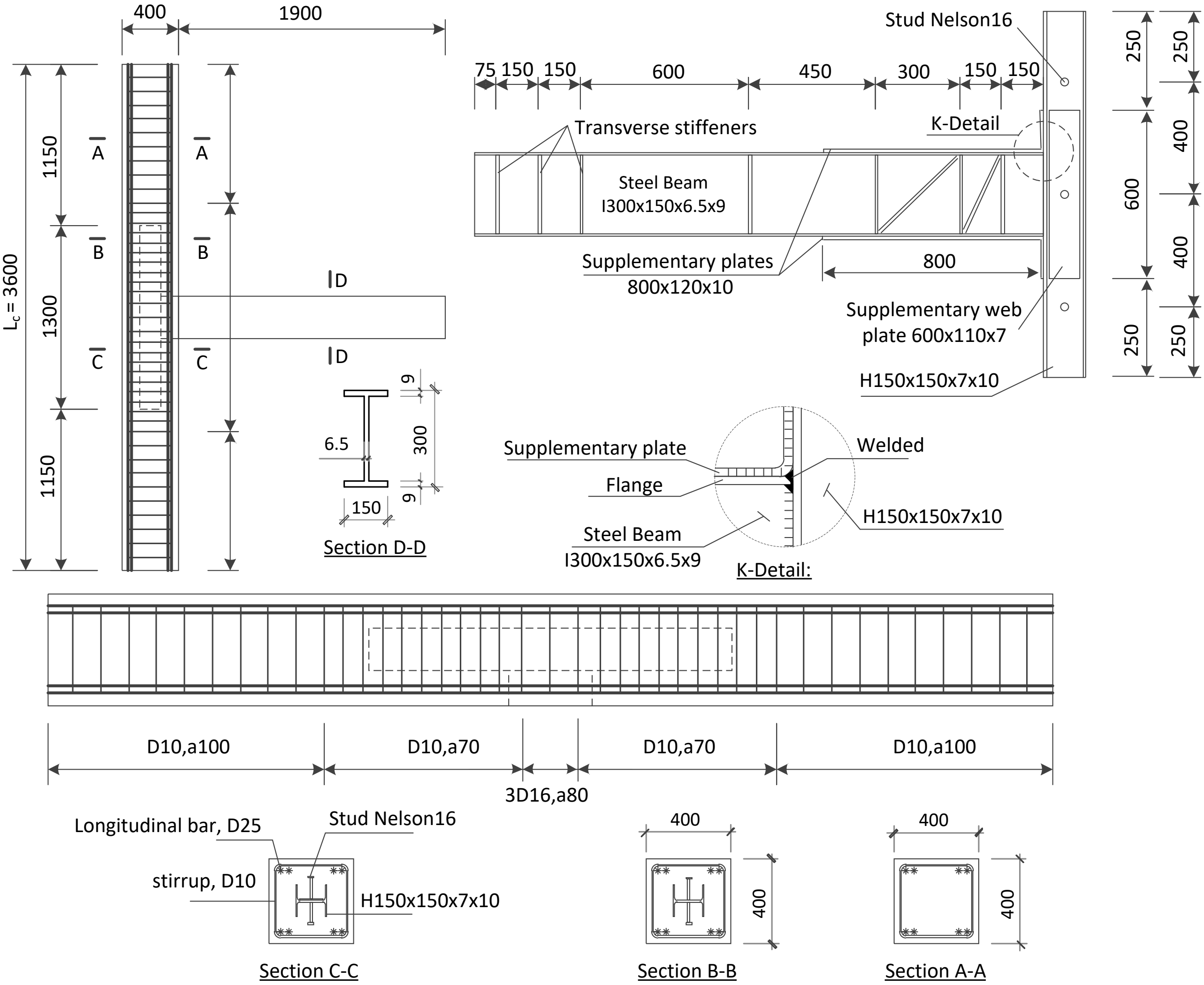

Fig. 1 Specimen description (unit in mm)

Fig. 2 Steel fibers used in FRC joint

Besides, Saghafi *et al.* (2018) revealed that fiber reinforced cementitious composite connections considerably enhanced the shear and flexural capacity as well as the deformation and damage tolerance behavior at post-cracking stage in comparison with those of normal concrete connections at ultimate stages. The results indicated that FRC with 1.2% to 2% volumetric steel fibers (hooked - end type) can be used as an alternative to part of confining reinforcement in joint regions. Fibers provide the better distribution of both internal and external stresses due to the formation of a three dimensional reinforcing network.

However, few experimental studies have been implemented to investigate the influence of FRC on the behavior of RCS type joint. This paper represents an experimental study on seismic performance of RCS joints proposed in Smartcoco project (Smartcoco 2017, Somja *et al.* 2018). Two full scale exterior composite joints with and without SFRC were tested under reversed cyclic loading. Seismic behaviors of specimens were evaluated and compared in terms of load bearing capacity, story drift capacity, energy dissipation, and stiffness degradation.

2. Details of specimens

2.1 Geometry

The specimens, designed according to the tentative design method proposed within project Smartcoco, are full-scale exterior RCS joints. Each specimen consists of a steel profile which is directly welded to the steel beam. Two test joints with the same size and geometry shape were

Table 1 Mix proportion for normal concrete and SFRC (kg/m^3)

Particulars	Normal concrete	SFRC
Portland Cement 40	420	413
Coarse sand 20 mm	947	932
Fine sand 3,5 mm	618	609
Fly ash Class F	170	167
Water	179	176
Polycarboxylate R-209	6.7	6.6

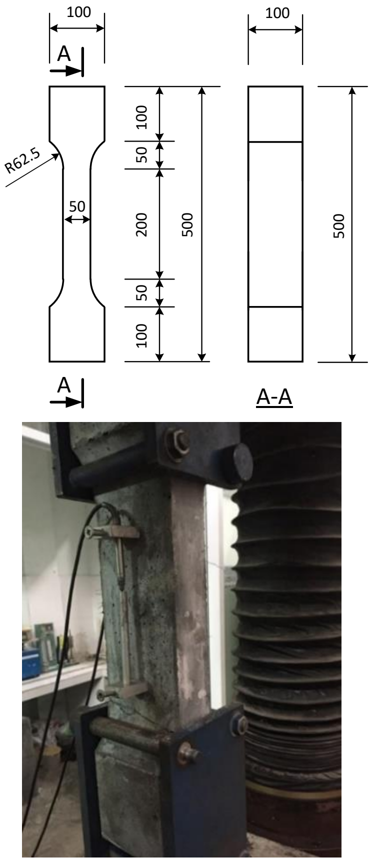

Fig. 3 Specimen geometry and tension test setup (unit in mm)

evaluated in this paper. The first one, called RC joint, has been casted by normal concrete while the second one, called FRC joint, has been casted by SFRC in the whole column. The dimension of specimen is shown in Fig. 1.

The design rule has to follow the “strong column-weak beam” philosophy. However, one of the objective of this experimentation was to study the behavior of the “shear key” (embedded steel profile) under cyclic load. Therefore, the steel beam was reinforced with stiffeners in order to make sure that the failure mode of the test specimen does not caused by the beam yielding.

2.2 Materials used

The RC joint specimen was constructed using normal weight, ready mixed concrete and self-compacting. The fly ash is used as a supplementary cementitious material in the production of Portland cement concrete. In this study, the ASTM Class F fly ash (ASTM 2017) from Pha Lai Power Station, Vietnam has been used. For the FRC joint, end-hooked steel fibers of 30 mm long and 0.5 mm diameter were used into the concrete mix (Fig. 2). In this study, we concentrated only on the influence of presence of fibers and ignored the influence of distribution or orientation of fibers.

Table 2 Properties of normal concrete and SFRC)

Property	Normal concrete	SFRC
Compressive strength (MPa)	37	43
Tensile strength (MPa)	2.4	3.8
Modulus of elasticity (GPa)	32.5	33.7
Average density (kg/m^3)	2340	2422
Slump flow (mm)	570	552

Table 3 The profiles and steel bars strengths derived from experiments

Item	fy [MPa]	fu [MPa]
H profile	294	436
I profile	285	420
Steel bar D25	412	569
Steel bar D16	336	485
Steel bar D10	354	496

In this investigation, a fiber content of 1.5% volume with ultimate tensile strength of 1000 MPa has been selected The details of mix proportions of specimens are given in Table 1.

The compressive strength of normal concrete and SFRC were found based on the average value of compressive tests carried out on standard cylinders (150 mm × 300 mm). The uniaxial tension tests have been conducted by using the dog bone shaped specimens (Yoo *et al.* 2016). The tension tests revealed that the tensile strength of SFRC (3.8 MPa) is 1.58 times as that of normal concrete (2.4 MPa).

Details about the properties of normal concrete and SFRC can be found in Table 2.

The yield stress fy and ultimate stress fu in tensile tests are reported for the structural reinforcing steel components in Table 3.

2.3. Specimen preparation

The specimens were constructed and casted at the Construction Materials Laboratory of University of Transport and Communications, Vietnam. In the beginning, the steel beam is welded to H profile. Then, they were placed in the mold along the reinforcement cage. Finally, the normal concrete was filled into the mold. In this experiment, concrete was designed as self-compacting. For FRC joint, the mechanical vibrator was used to ensure that SFRC was filled properly at the joint area.

2.4. Instrumentation

Several different instruments were used in the testing of the specimens, such as displacement transducers (LVDTs) for measuring displacements, load cells for measuring applied forces and reactions, and strain gauge for recording


Fig. 4 Manufacture of specimens


Fig. 7 Specimen before the test

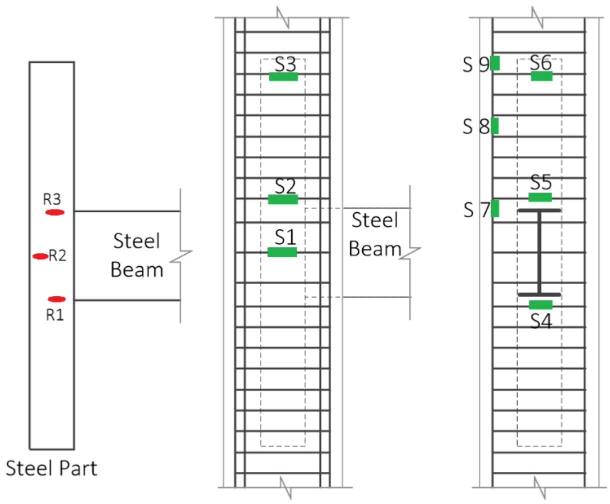

Fig. 5 Strain gauge location

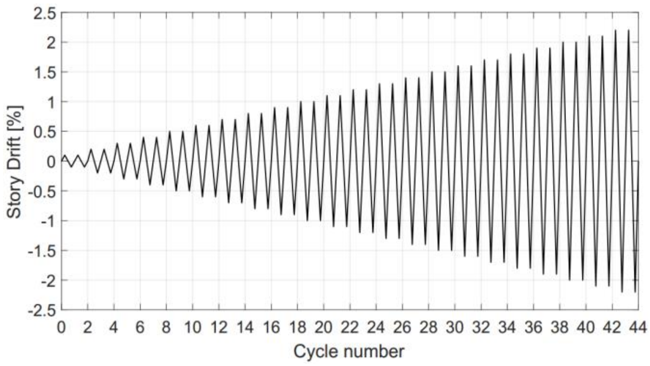

Fig. 8 Loading procedure

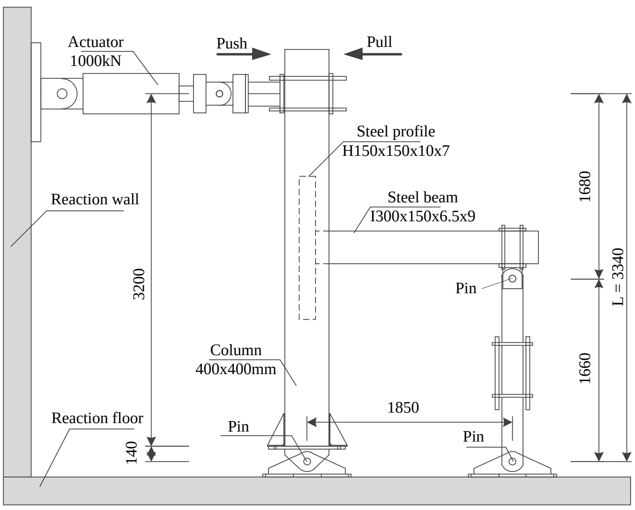

Fig. 6 Schema of testing

strains. At the joint area, nine strain gauges, noted from S1 to S9, were placed on reinforcements of the column as shown in Fig.5. There were also three strain gauge rosettes, noted from R1 to R3, which were arranged in the encased steel profile.

3. Test setup

The test setup is shown in Figs 6 and 7. The bottom of the column was pinned to the strong floor of laboratory. The hydraulic actuator was horizontally held to the strong wall. This actuator with the capacity of 1000 kN and the stroke length of 150 mm was used to apply the cyclic lateral displacement at the top of column. Due to the technical reason, there was no axial force acting on the column.

The lateral displacement was imposed cyclically, in a quasi-static way, at the top of the column. (Fig. 8). This loading protocol is defined according to the conventional limit of elastic range δy which was estimated in this study by a numerical simulation.

The loading cycle consisted of a series of reversed displacement cycles of incremental displacement amplitude δy. It is accordance to Recommended testing procedure for assessing the behavior of structural steel elements under cyclic loads by European Convention for Constructional Steelwork (ECCS 1986). To reflect the cumulative damage, each drift step consisted of 2 cycles of pushing and pulling.

4. Experimental results

4.1. Failure modes

During the test, the cracks were identified in the

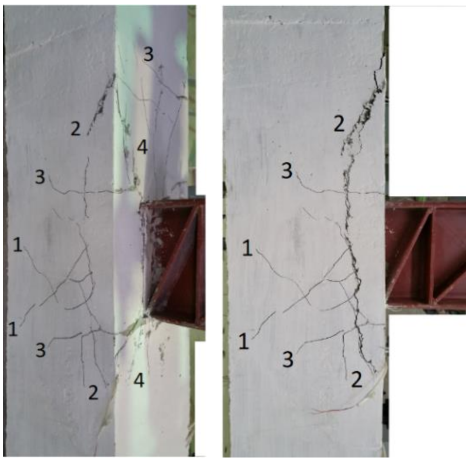

Fig. 9 Damage of RC joint

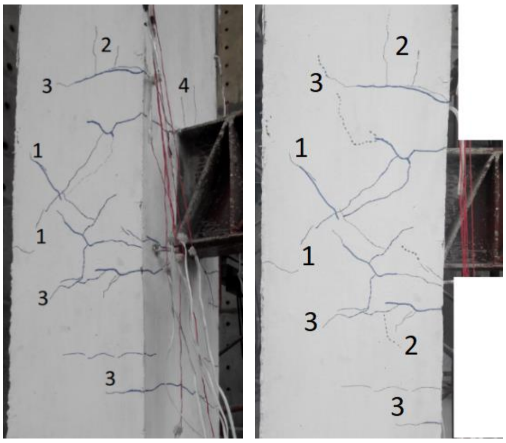

Fig. 10 Damage of FRC joint

specimens and marked with pen. The cracks have been detected in each step by observation because the loading shouldn't be stopped to measure the crack width. In general, the damage of two specimens was quite different. Fig. 9 and Fig. 10 shows that there were more cracks in FRC joint. However, the width of these cracks was limited and the concrete wasn't crushed from FRC specimen. Contrarily, some diagonal and vertical cracks were opened in RC joint. At final stage, the concrete of RC joint was crushed locally.

Four types of cracks were identified in RC joint, including:

- diagonal cracks on two lateral faces at the center of the joint region (type 1)
- inclined and horizontal cracks outside joint region (type 2)
- horizontal cracks on four faces of the column (type 3)
- vertical cracks on the front face (type 4)

The first damage was a diagonal crack (type 1) at 0.8% drift due to joint panel shear. At 0.9% drift, the horizontal and inclined cracks (type 2) originated at the steel beam flanges were observed. Another diagonal crack (type 1) was formed symmetrically in the joint at 1.2% drift along with some horizontal cracks in the column (type 3). Some vertical cracks (type 4) were appeared from the top flange and propagated upward in the RC column zone at 1.4% drift. At 1.7% drift, a vertical crack connected with two symmetric cracks of type 2 was appeared. Then, this crack propagated and widened gradually. Finally, the concrete was crushed around the end of encased steel profile.

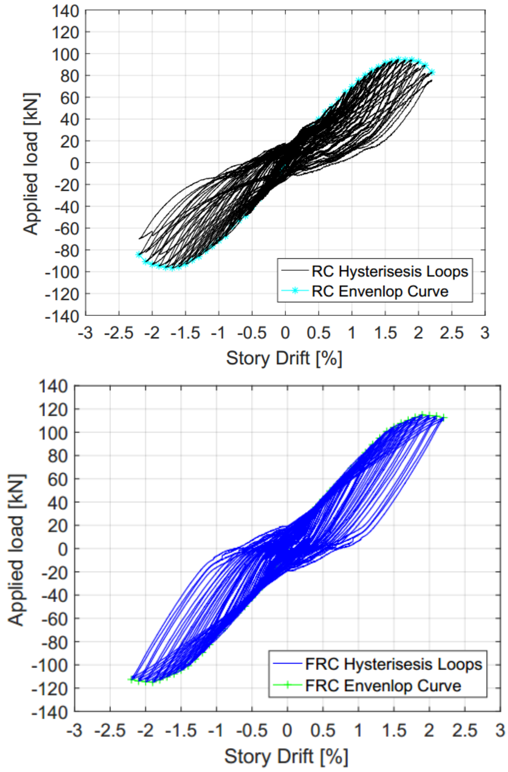

Fig. 11 Load- story drift relationship

Similar to RC joint, the first crack appeared in FRC joint was type 1 due to joint panel shear. However, the appearance of this crack was at the higher drift value (1% drift). After that, some horizontal cracks (type 2) were also formed from the flange of steel beam. At 1.3% drift, the first horizontal flexural crack (type 3) was identified on the face of column.

Comparing to RC joint, the vertical cracks (type 4) were shorter. It shows that the presence of steel fibers helps to reduce the width of crack patterns in FRC joint. This interesting finding was resulted from the fact that the load was transferred more effectively from the joint region to the column in FRC specimen. That led to less deformation in the joint region of FRC specimen. Consequently, the concrete was not crushed locally at this region.

4.2. Load-displacement

Fig. 11 represents the typical load- story drift plot of RC joint and FRC joint tested under cyclic loading. As can be seen, hysteretic loops were full and approximately symmetric for both specimens. The pinching effect was also found in both joints but it was clearer in RC joint than in FRC joint.

Fig. 12 shows the envelope curves which were obtained by interconnecting the peak values of all cycles. The load-story drift curve of FRC joint and RC joint can be divided in three stages. The first stage (from 0 to 1% drift) was represented by the elastic behavior period in which some micro cracks were detected. In the second stage (from 1%

Table 4 Yielding, limit and final points

Item	δ_y (%) Yielding point	P_y (kN) Yielding point	$\delta_{\max}$ (%) Limit point	P_{max} (kN) Limit point	$P_{DR=2.2\%}$ (kN) Final point
RC joint	1.37	86.5	1.7	94.63	82.94
FRC joint	1.53	105.4	1.9	114.86	112.54

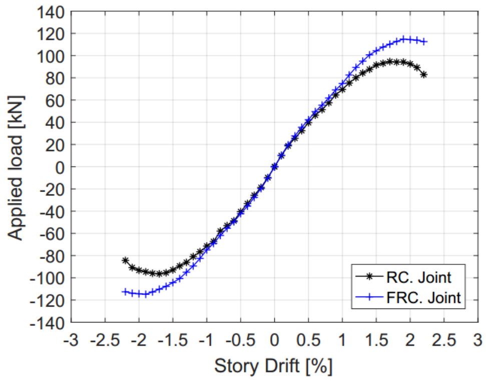

Fig. 12 Load- story drift plot

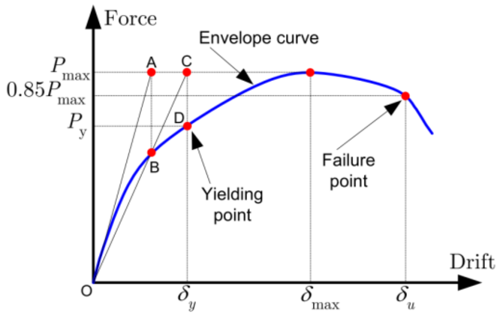

Fig. 13 Definition of yielding point

to 2% drift), these micro cracks were propagated and widened. Finally, the third stage was marked by the deterioration of joint strength with the development of cracks.

It was observed that this envelope curve was quite similar for both FRC and RC joints in the first stage. In the second stage, the FRC joint reached the limited point (at 1,9% drift) after RC joint reached the limited point (at 1,7% drift). Their maximum loads are 114.86 kN and 94.63 kN for FRC joint and RC joint, respectively. It confirms that the presence of steel fibers has increased the load carrying capacity and stiffness of specimens.

4.3. The yielding point

The envelope curves of the hysteresis loops are shown in Fig. 12. The yield displacement of specimen is determined using the general yielding method proposed by Li *et al.* (2013). As shown in Fig. 13, point D is the yielding point.

Table 4 shows the drifts and corresponding horizontal applied loads at yielding, limit and final points of two specimens. It is noted that the RC joint was yielded at about

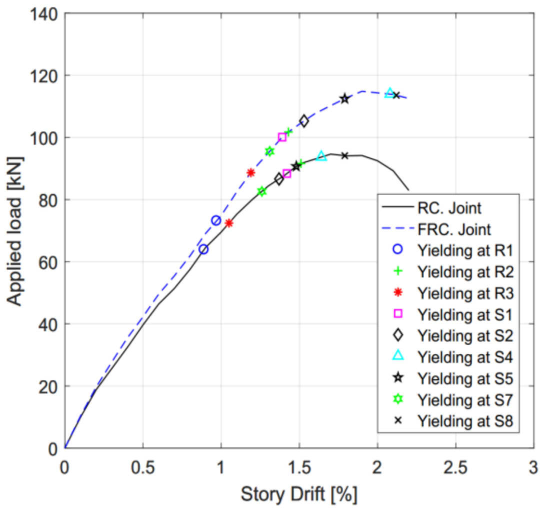

Fig. 14 Load-drift envelope curves and yielding points

1.37% drift and 86.5 kN of applied load. That means the yielding of RC joint was detected early than that of FRC joint where the correspondent drift and the applied load were 1.53% and 105.4kN, respectively. At the final stage, the applied load decreases to 112.54 kN for FRC joint and 82.94 kN for RC joint. It indicates that the strength degradation ratio was about 1.6% for FRC joint and 12.3% for RC joint. Besides, the ratio between the maximum force and the yielding force is about 1.1 for both RC joint and FRC joint.

4.4. Strain analysis

Fig. 14 and Table 5 show the comparison between RC joint and FRC joint in terms of yielding points during the loading. For both specimens, the yielding was detected in the encased profile by strain gauge rosettes R1, R3 before it was detected in the reinforcements by strain gauges S1, S2, S7.

In RC joint, the encased profile and the reinforcement were yielded at the drift level of 0.89% and 1.26%, respectively. In FRC joint, these yielding points had the drift level of 0.97% and 1.31%. This fact affirmed that the FRC joint with steel fibers was yielded later than RC joint. It was also found out that in the joint region (strain gauges R2, S1) and next to the flange of steel beam (strain gauges S4, S5), the yielding of SFRC specimen appeared after it was detected in RC specimen. This was in accordance with the damage state observed during the experiment.

4.5. Energy dissipation

Energy dissipation capacity is the important characteristic affecting the structure's seismic performance. It can be estimated from area within the load- displacement curves for every cycle of load.

Fig. 15 presents the definition of the dissipated energy of one hysteresis loop and the maximum dissipated energy which could be theoretically dissipated within the same load and displacement limits, assuming a perfectly plastic response. As can be seen, the dissipated energy is black

Table 5 The yielding values

		R1	R2	R3	S1	S2	S4	S5	S7	S8
RC joint	Drift (%)	0.89	1.51	1.05	1.42	1.37	1.64	1.48	1.26	1.79
	Applied load (kN)	63.87	91.63	72.44	88.39	88.64	93.68	90.7	82.64	94.14
FRC joint	Drift (%)	0.97	1.43	1.19	1.39	1.53	2.08	1.79	1.31	2.12
	Applied load (kN)	73.14	101.75	88.67	100.1	105.3	113.95	112.48	95.54	113.59

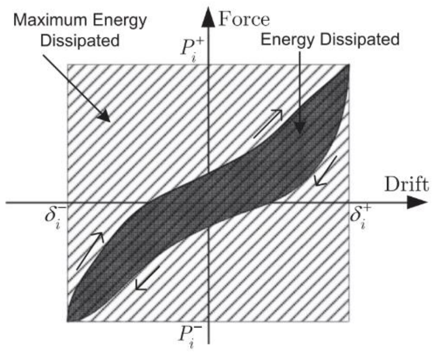

Fig. 15 Definition of energy dissipated and maximum energy dissipated

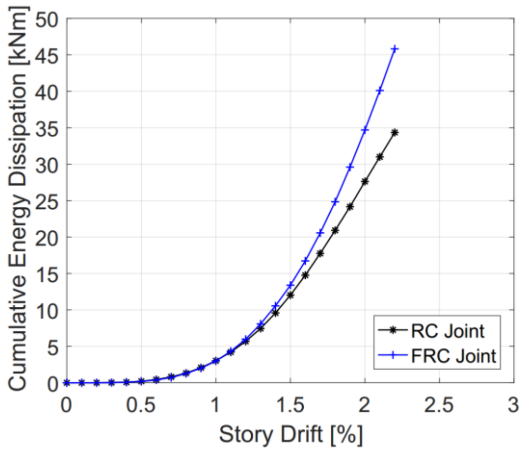

Fig. 16 Variation of the cumulated dissipated energy

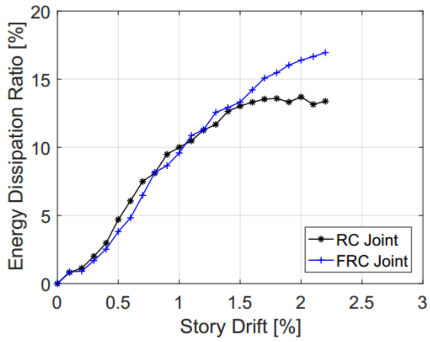

Fig. 17 Energy dissipation ratio

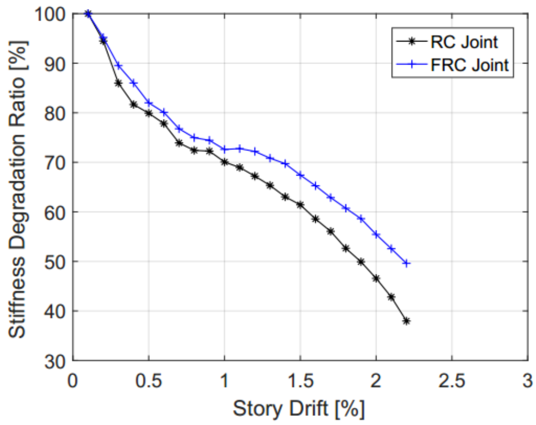

Fig. 18 Stiffness degradation

solid hatched quantity.

Cumulative energy dissipation is calculated by summing energy dissipated in previous cycles. Fig. 16 shows the cumulative dissipated energy at each displacement level. It can be observed that there was a significant difference between the behavior of RC joint and FRC joint. The dissipated energy of RC joint changes gradually following the increase of drift while dissipated energy of FRC joint increases rapidly from the turning point of dissipated energy where the story drift is equal to 1.2%. At the final stage, FRC joint was able to dissipate the larger amount of energy than RC joint was by 30%.

Fig. 17 shows the dissipated energy ratio at each displacement level. The energy dissipation ratio was calculated as the ratio between the effective dissipated energy during each loading cycle and the maximum theoretical dissipated energy. This index indicates the structural performance in energy-based seismic design. The experimental results demonstrated that there was no major difference in energy dissipation ratio during each step until the drift reaching to 1.5%. From this drift level to the end of the test, the energy dissipation ratio appeared stably in RC joint while it still increased gradually in FRC joint.

Tables 6 and 7 shows differences values of the energy dissipation during the test for two specimens.

4.6. Stiffness degradation

The stiffness of elements is defined as the load which induces a unit deflection in a given direction at a specified point. This definition is based on a linear relationship between load and deflection. In civil engineering, the stiffness of structural members (K) is defined as the ratio between the applied load and the resulting deflection. Fig. 18 shows that the stiffness charts of joints in two tested specimens decreased at the same rate in the first stage (from 0 to 1% drift). After that, the stiffness of RC joint decreased more rapidly than that of FRC joint due to the opening of cracks.

Table 6 Experimental results of RC specimen

Displacement (m)	Story drift (%)	Applied load (kN) Push	Pull	Maximum dissipated energy (kNm)	Energy dissipation (kNm)	Energy dissipation ratio (%)
(1)	(2)=(1)/L	(3)	(4)	(5)=[(1)+(1)]*[(3)-(4)]	(6)	(7)=(6)/(5)
0.0034	0.1	9.93	-9.80	0.134	0.0011	0.82
0.0068	0.2	18.77	-18.65	0.509	0.0058	1.14
0.0102	0.3	25.61	-25.73	1.047	0.021	2.01
0.0136	0.4	32.44	-33.15	1.784	0.053	2.97
0.017	0.5	39.67	-39.80	2.702	0.127	4.70
0.0204	0.6	46.36	-46.50	3.789	0.231	6.10
0.0238	0.7	51.37	-52.30	4.935	0.372	7.54
0.0272	0.8	57.52	-57.97	6.282	0.513	8.17
0.0306	0.9	64.58	-64.60	7.906	0.752	9.51
0.034	1	69.56	-70.10	9.497	0.952	10.02
0.0374	1.1	75.32	-76.52	11.357	1.191	10.49
0.0408	1.2	80.09	-80.93	13.139	1.484	11.29
0.0442	1.3	84.34	-86.10	15.067	1.764	11.71
0.0476	1.4	87.62	-89.34	16.847	2.132	12.66
0.051	1.5	91.47	-92.88	18.804	2.451	13.03
0.0544	1.6	93.05	-95.43	20.506	2.733	13.33
0.0578	1.7	94.63	-96.41	22.084	2.993	13.55
0.0612	1.8	94.08	-95.96	23.262	3.162	13.59
0.0646	1.9	94.18	-94.63	24.395	3.253	13.33
0.068	2	92.49	-93.24	25.259	3.461	13.70
0.0714	2.1	89.27	-90.77	25.709	3.383	13.16
0.0748	2.2	82.94	-84.36	25.028	3.352	13.39

Table 7 Experimental results of FRC specimen

Displacement (m)	Story drift (%)	Applied load (kN) Push	Pull	Maximum dissipated energy (kNm)	Energy dissipation (kNm)	Energy dissipation ratio (%)
(1)	(2)=(1)/L	(3)	(4)	(5)=[(1)+(1)]*[(3)-(4)]	(6)	(7)=(6)/(5)
0.0034	0.1	10.31	-10.35	0.141	0.0012	0.87
0.0068	0.2	19.64	-19.86	0.537	0.0049	0.91
0.0102	0.3	27.70	-27.98	1.136	0.0191	1.68
0.0136	0.4	35.48	-35.66	1.935	0.049	2.52
0.017	0.5	42.28	-42.41	2.880	0.11	3.81
0.0204	0.6	49.56	-49.76	4.052	0.195	4.82
0.0238	0.7	55.41	-55.67	5.288	0.342	6.46
0.0272	0.8	61.85	-62.14	6.745	0.549	8.14
0.0306	0.9	69.09	-69.35	8.472	0.732	8.64
0.034	1	74.87	-75.06	10.195	0.976	9.57
0.0374	1.1	82.54	-82.84	12.370	1.342	10.85
0.0408	1.2	89.35	-89.7	14.610	1.647	11.27
0.0442	1.3	94.97	-95.51	16.838	2.111	12.53
0.0476	1.4	100.67	-101.32	19.229	2.477	12.88
0.051	1.5	104.28	-104.86	21.333	2.834	13.29
0.0544	1.6	107.69	-108.21	23.490	3.331	14.18
0.0578	1.7	110.23	-110.79	25.550	3.843	15.04
0.0612	1.8	112.73	-113.11	27.643	4.27	15.45
0.0646	1.9	114.86	-115.26	29.732	4.758	16.00
0.068	2	114.36	-114.79	31.164	5.1	16.36
0.0714	2.1	113.85	-114.32	32.583	5.417	16.62
0.0748	2.2	112.55	-113.24	33.778	5.71	16.90

5. Conclusions

The study has tested two full scale specimens to investigate the effect of SFRC on seismic performance of exterior RCS joints. Each tested RCS joint consisted of an H steel profile embedded inside RC column and directly welded to the steel beam. Both specimens had the same geometry but they were filled by different types of concrete. Based on the experimental results, it was found that the use of SFRC in column improved the performance of the RCS effectively. The FRC joint shown lower damage than RC joint did as there was no concrete crushed from FRC specimen. During the loading process, the FRC joint also shown the significant increase of load carrying capacity by 20% and the better ductility and energy dissipation capacity (30%) in comparison with the RC joint. Further experimental studies are needed to extend the range of test data and to investigate other parameters such as the type of fiber steel, and the fiber volume fraction. A numerical investigation would be also necessary to reduce the experimental cost.

Acknowledgments

This research is funded by Vietnam National Foundation for Science and Technology Development (NAFOSTED) under grant number 107.01-2016.06.

References

ASCE Task Committee on Design Criteria for Composite Structures in Steel and Concrete (1994), "Guidelines for design of joints between steel beam and reinforced concrete columns", *J. Struct. Eng*., **120**(8), 2330-2357. https://doi.org/10.1061/(ASCE)0733-9445(1994)120:8(2330).

ASTM C618-17a Standard Specification for Coal Fly Ash and Raw or Calcined Natural Pozzolan for Use in Concrete (2017), *ASTM*., West Conshohocken, U.S.A.

Deierlein, D.D. and Noguchi, H. (2004), "Overview of U.S. - Japan research on seismic design of composite reinforced concrete and steel moment frame", *J. Struct. Eng*., **130**(2), 361-367. https://doi.org/10.1061/(ASCE)0733-9445(2004)130:2(361).

Deierlein, G.G., Sheikh, T.M., Yura, J.A. and Jirsa, J.O. (1989), "Beam-column moment connections for composite frames: Part 2", *J. Struct. Eng*., **115**(11), 2877-2896. https://doi.org/10.1061/(ASCE)0733-9445(1989)115:11(2877).

Dong, J., Hui, Ma., Zhang, N., Liu, W. and Mao, Z. (2018), "Seismic damage assessment of steel reinforced recycled concrete column-steel beam composite frame joints", *Earthq. Struct*., **14**(1), 73-84. https://doi.org/10.12989/eas.2018.14.1.073.

ECCS, T. TWG 1.3 (1986), "Recommended testing procedure for assessing the behavior of structural steel elements under cyclic loads".

Fargier-Gabaldon, L. (2005), "Design of moment connections for composite framed structures", Ph.D. Dissertation, The University of Michigan, U.S.A.

Gefken, P.R. and Ramey, M.R. (1989), "Increased joint hoop spacing in type 2 seismic joints using fibre reinforced concrete", *ACI Struct. J*., **86**(2), 168-172.

Gong, J., Zou, X., Shi, H., Jiang, C. and Li, Z. (2018), "Numerical Investigation of the Nonlinear Composite Action of FRP-Concrete Hybrid Beams/Decks", *Appl. Sci*. **2031**. https://doi.org/10.3390/app8112031.

Jinjie, M., Yarong, Z., Zhifeng, G. and Qingxuan, S. (2015), "Experimental research on seismic behavior of a composite RCS frame", *Steel Compos. Struct*., **18**(4), 971-983. https://doi.org/10.12989/scs.2015.18.4.971.

Kanno, R. and Deierlein, D.D. (2002), "Design Model of Joints for RCS Frames", *The Proceeding of Composite Construction in Steel and Concrete IV*, Alberta, Canada.

Kalaivani, M. and Karthik, A. (2016), "Steel fibre reinforced concrete beam-column joint - A review", *Int. J. Eng. Res. Technol*., **5**(5), 166- 173.

Li, B., Lam, E.S., Wu, B. and Wang, Y. (2013), "Experimental investigation on reinforced concrete interior beam-column joints rehabilitated by ferrocement jackets", *Eng. Struct*., **56**, 897-909. https://doi.org/10.1016/j.engstruct.2013.05.038.

Li, W., Li, Q.N., Jiang, W.S. and Jiang, L. (2011), "Seismic performance of composite reinforced concrete and steel moment frame structures - state-of-the-art", *Compos. Part B: Eng*., **42**(2), 190-206. https://doi.org/10.1016/j.compositesb.2010.10.008.

Mirghaderi, S., Eghbali, N. and Ahmadi, M. (2016), "Moment connection between continuous steel beams and reinforced concrete column under cyclic loading", *J. Construct. Steel Res*., **118**, 105-119. https://doi.org/10.1016/j.jcsr.2015.11.002.

Nguyen, X.H., Nguyen, Q.H, Le, D.D and Mirza, O. (2017), "Experimental study on seismic performance of new RCS connection", *Struct*., **9**, 53-62. https://doi.org/10.1016/j.istruc.2016.09.006.

Nguyen, X.H., Nguyen, Q.H. and Le, D.D. (2019), "Static behavior of novel RCS through-column-type joint: Experimental and numerical study", *J. Steel Compos. Struct*., **32**(1), 111-126. https://doi.org/10.12989/scs.2019.32.1.111.

Nishiyama, I., Kuramoto, H. and Noguchi, H. (2004), "Guidelines: seismic design of composite reinforced concrete and steel buildings", *J. Struct. Eng*., **130**(2), 336-342.

Oinam, R.M., Kumar, P.C. and Sahoo, D.R. (2019), "Cyclic performance of steel fiber-reinforced concrete exterior beam-column joints", *Earthq. Struct*., **16**(5), 533-546. https://doi.org/10.12989/eas.2019.16.5.533.

Parra-Montesinos, G. and Wight, J.K. (2010), "Seismic response of exterior RC column-to-steel beam connections", *J. Struct. Eng*., **126**(10), 1113-1121. https://doi.org/10.1061/(ASCE)0733-9445(2000)126:10(1113).

Degée, H., Plumier, A., Bogdan, T., Popa, N., Cajot, L.G., De Bel, J.M. and Elghazouli, A. (2016), "Smart composite components-concrete structures reinforced by steel profiles", SmartCoCo. European Commission, Research Programme of the Research Funds for Coal and Steel, TGS, 8.

Somja, H., Hjiaj, M., Nguyen, Q.H., Plumier, A. and Degee, H. (2018), "The SMARTCOCO design guide for hybrid concrete-steel structures", The *Proceedings of the 12th International Conference on Advances in Steel-Concrete Composite Structures, Valencia*, Spain, June.

Yoo, D.Y., Shin, H.O. and Yoon, Y.S. (2016), "Ultrasonic monitoring of setting and strength development of ultra-high-performance concrete", *Mat*., **9**(4), 294. https://doi.org/10.3390/ma9040294.

Zhang, X., Jiawei, Z., Xuejian, G. and Shaohua, Z. (2018), "Seismic performance of prefabricated high-strength concrete tube column-steel beam joints", *Advan. Struct. Eng*., **21**(5), 658-674. https://doi.org/10.1177/1369433217726895.

AT